PERGAMON

International Journal of Solids and Structures 37 (2000) 1211–1243

INTERNATIONAL JOURNAL OF SOLIDS and STRUCTURES

www.elsevier.com/locate/ijsolstr

Limit analysis of the bearing capacity of fissured materials

X. Zheng, J.R. Booker, J.P. Carter*

Department of Civil Engineering, The University of Sydney, NSW 2006, Australia

Received 11 June 1998; in revised form 7 September 1998

Abstract

Formulations for the upper and lower bound theorems of plasticity are presented for fissured soil and jointed rock. The methods ignore elastic deformations and are based on the assumption that the fissured soil or rock mass can be treated as an anisotropic, rigid-plastic continuum. In the upper bound formulation, velocity discontinuity multipliers are introduced to deal with the discontinuities in the velocity field. For both the upper and lower bound formulations, linearized failure surfaces for the fissured materials are developed. The illustrative examples indicate that the new procedures are very efficient even when a quite coarse mesh is used to represent the mass of failing material, and that the 'exact' failure loads are always bracketed by the upper bound and lower bound calculations. Moreover, by increasing the number of planes in the failure surface or/and refining the meshes, the accuracy of the bounds is raised.

1. Introduction

Natural soil and rock deposits often have a history which involves a wide range of stress states. This can include overstressing and also tensile failure of such geo-materials and so may result in extensive fissuring or jointing of the medium. Such defects occur as physical discontinuities within the matrix material, and hence, the mechanical behaviour of these rock and soil masses is governed not only by the intact matrix material but also by the characteristics of the discontinuities. The presence of defects in the material often gives rise to numerical difficulties during engineering analysis of these materials. However, if the fissures in each set are reasonably constant in orientation and closely spaced, then the overall mass can be treated as an anisotropic continuum for the purpose of mechanical analysis. The properties of this composite material are determined by the defect strength, the strength of the intact matrix, and the orientations of the defect sets. Examples of the engineering analysis of fissured materials using this approach appear in papers by Davis (1980), Alehossein et al. (1992), Lav et al. (1995) and Zheng and Booker (1997). All these studies reached similar conclusions, i.e., that the presence of weak fissures and joints significantly reduces the bearing capacity of shallow foundations.

* Corresponding author. Fax: +61-2-9351-3343.
E-mail address: j.carter@civil.usyd.edu.au (J.P. Carter).

0020-7683/00/$ - see front matter
PII: S0020-7683(98)00282-0

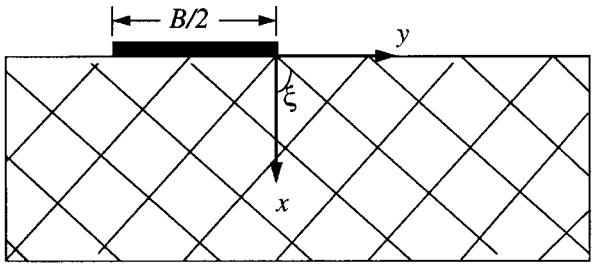

Fig. 1. Footing on a fissured material.

Limit analysis techniques, such as the upper and lower bound methods of the theory of plasticity, have proved to be the most effective methods for predicting plastic collapse in many areas of soil and rock mechanics. They have been used previously to solve complex problems that involve anisotropy and non-homogeneity of soil or rock. As will be demonstrated, they also provide a powerful approach for studying the behaviour of fissured materials. For example, Chen (1975) applied limit analysis to the bearing capacity of footings on a single layer and two-layer soils, exhibiting both anisotropy and non-homogeneity. His analysis was based on the assumption of a circular failure surface. Reddy and Venkatakrishna (1982), by adopting a Prandtl-type failure mechanism, applied the upper bound theorem to obtain the bearing capacity of a strip footing on cohesive–frictional soils exhibiting anisotropy and non-homogeneity in cohesion. Sloan, (1988) presented a technique, which computes a statically admissible stress field via finite elements and linear programming, for computing lower bound limit loads under conditions of plane strain. His results show that the solution is a strict lower bound on the true collapse load. By using the upper bound theory, Michalowski (1993) found that the limit analysis method is a convenient method for calculating the bearing capacity in cases where the soil strength increases with depth. Sloan and Kleeman (1995) proposed a quite general upper bound method which permits a large number of discontinuities in the velocity field and can be applied to both homogeneous and non-homogeneous materials whose strength is cohesive–frictional, or purely cohesive. Yu and Sloan (1997) have applied the limit theorems to reinforced soils and found that a major advantage of these methods is that the complex loading, geometry and soil behaviour can all be dealt with in a straightforward manner.

The purpose of this paper is to use the limit analysis method to develop a general numerical approach for finding the lower bound and upper bound solutions to the bearing capacity of a smooth or rough rigid strip footing resting on fissured soil or rock (Fig. 1). To achieve this objective, the formulations developed for both lower and upper bound solutions assume that the failure criterion for a fissured material can be linearized. Elastic deformations are ignored and it is assumed that a fissured material can be treated as an anisotropic continuum. A number of applications are given to illustrate that the formulations are computationally efficient and give good estimates of the true limit loads, even with a relatively coarse computational grid. Detailed comparisons with results obtained from the method of characteristics (Zheng and Booker, 1997) are also presented. The illustrative examples indicate that by increasing the accuracy of the linearized failure criterion and by refining the mesh sizes, the numerically obtained upper and lower bounds more closely bracket the exact collapse load.

2. Statement of the problem

The development of failure criteria for materials with regular sets of fissures has been presented previously by a number of authors, e.g. Davis (1980), Zheng and Booker (1997). For completeness, the

formulation of the failure surface for a cohesive–frictional material with either a single set of fissures or two sets of fissures is presented in Appendix B.

Consider a plastic body occupying a volume V with a surface S. Suppose that a portion of the surface S_L is loaded while the remainder of the surface is subjected to zero tractions or velocities, and hence zero power.

For two-dimensional problems, the bound theorems allow determination of upper and lower bounds of the quantity $\int_{S_L}(T_x u + T_y \upsilon)\,\mathrm{d}S$, which is the power input to S_L. (T_x, T_y) are the components of the traction and (u, υ) are the velocity components along S_L. The power input may be used to calculate the upper and lower bounds in a number of cases, as indicated below.

If S_L is a straight portion of the boundary, corresponding to the interface with a rigid footing that is subjected to a normal velocity Π and zero tangential displacement, then it is clear that

$$\int_{S_L}\left(T_x u + T_y \upsilon\right)\mathrm{d}S = \Pi P_{rn}$$

where P_{rn} is the normal force on the rough rigid footing. Similarly, if a straight portion of the boundary is subjected to a normal velocity Π, but is shear free, then

$$\int_{S_L}\left(T_x u + T_y \upsilon\right)\mathrm{d}S = \Pi P_{sn}$$

where P_{sn} is the normal force on the smooth rigid footing.

The zero power condition on the remainder of the boundary includes many possibilities and some of these are:

1. Traction free, i.e. $T_x = 0$, $T_y = 0$,
2. Zero velocity, i.e. $u = 0$, $\upsilon = 0$.

The boundary S–S_L can be made up of a combination of these conditions.

3. Formulation of the upper bound problem

The upper bound theorem is a powerful tool for stability analysis and has been widely used in many areas of goetechnical design. General formulations of the upper bound theorem use finite elements and linear programming (e.g. Sloan and Kleeman, 1995). The conditions required to establish an upper bound solution to the collapse load are essentially as follows:

The loads, determined by equating the external work to the internal dissipation in an assumed velocity field that satisfies (a) the velocity boundary conditions and (b) the strain and velocity compatibility conditions, are not less than the actual collapse load.

Thus, the upper bound technique considers only velocity, failure modes and energy dissipation. The stress distribution need not be in equilibrium, and is only defined in the deforming regions of the body. Hence, the constraints in the problem will be imposed on velocities by the plastic flow rule, velocity discontinuities and velocity boundary conditions. Once the solution to the upper bound linear programming problem has been found, a rigorous upper bound on the exact collapse load is found by equating the work of the external forces to the dissipation of internal power. It has been demonstrated in the limit theorems of plasticity theory that the stress and velocity fields are unique and complete if the material follows an associated flow rule. Accordingly, it is assumed that the material obeys an associated flow rule in this paper.

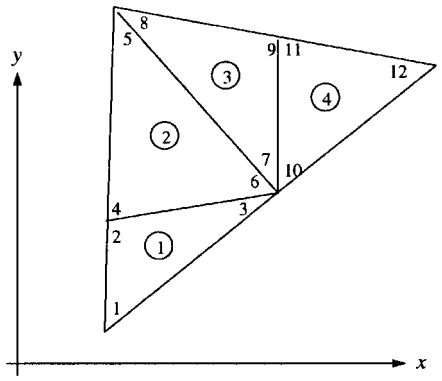

Fig. 2. Mesh of linear triangles for limit analysis.

The formulation in this section generalises the active set upper bound formulation of Sloan and Kleeman (1995) to permit a large number of discontinuities in the velocity field. Their method is based on a linear three-noded triangle with six unknown nodal velocities, a fixed number of unknown plastic multipliers and a fixed number of unknowns to describe the tangential velocity jumps along the length of a discontinuity. In the formulation presented here, it is also assumed that a velocity discontinuity may occur at any edge shared by a pair of adjacent triangles, and each discontinuity is typically defined by four nodes. A new feature in this formulation is the introduction of the velocity discontinuity multiplier, which plays a similar role to the tangential velocity jump (Sloan and Kleeman, 1995). Along a discontinuity, there are four unknown velocity discontinuity multipliers.

Assume that the rigid plastic region can be divided into triangular elements, as shown in Fig. 2, and that within an element there are six velocity components (Fig. 3) which are assumed to vary linearly according to

$$u = \sum_{i=1}^{3} N_i u_i,$$

$$v = \sum_{i=1}^{3} N_i v_i, \tag{1}$$

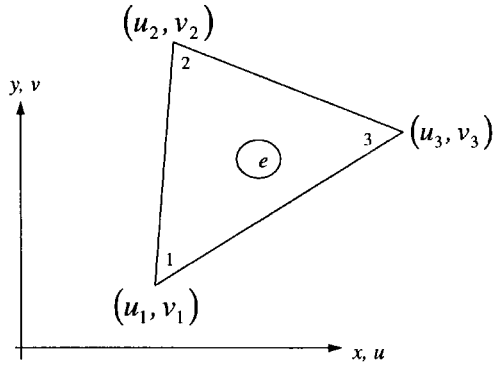

Fig. 3. Triangular element for upper bound limit analysis.

where u_i and v_i are the nodal velocities in the x- and y-directions, respectively, and N_i are linear shape functions, as defined in eqns (A1) of Appendix A.

3.1. Constraints for plastic flow in a continuum

For plane strain deformation of a rigid plastic material, the failure condition can be defined as:

$$f(\sigma_{xx}, \sigma_{yy}, \sigma_{xy}) = 0 \tag{2}$$

in which $(\sigma_{xx}, \sigma_{yy}, \sigma_{xy})$ are the planar stress components and the flow rule takes the following form:

$$\dot{\varepsilon}_{xx} = \dot{\lambda}\frac{\partial f}{\partial \sigma_{xx}} = -\frac{\partial u}{\partial x}$$

$$\dot{\varepsilon}_{yy} = \dot{\lambda}\frac{\partial f}{\partial \sigma_{yy}} = -\frac{\partial v}{\partial y}$$

$$\gamma_{xy} = \dot{\lambda}\frac{\partial f}{\partial \sigma_{xy}} = -\left(\frac{\partial u}{\partial y} + \frac{\partial v}{\partial x}\right) \tag{3}$$

where $\dot{\lambda} \geqslant 0$ is a plastic multiplier and u and v are the velocity components defined previously.

In order to formulate the problem as a linear programming problem, the failure surface has to be given by a linear function or linear functions. Following the discussion given in Appendix B for a material with vertical and/or horizontal fissures, the linearized failure functions take the following form:

$$f_j = A_{xx}^{(j)}\sigma_{xx} + A_{yy}^{(j)}\sigma_{yy} + 2A_{xy}^{(j)}\sigma_{xy} - G^{(j)} = 0, \quad j = 1, \ldots, J, \tag{4}$$

where $A_{xx}^{(j)}$, $A_{yy}^{(j)}$, $A_{xy}^{(j)}$, $G^{(j)}$ $(j = 1, \ldots, J,)$ are defined in eqns (B9), (B10) and (B12). Eqns (3) impose three equality constraints on the nodal velocities and plastic multipliers for each element, so that the plastic strain rates are given by

$$\dot{\varepsilon}_{xx} = -\frac{\partial u}{\partial x} = \dot{\lambda}\frac{\partial f}{\partial \sigma_{xx}} = \sum_{j=1}^{J}\dot{\lambda}_j\frac{\partial f_j}{\partial \sigma_{xx}} = \sum_{j=1}^{J}\dot{\lambda}_j A_{xx}^{(j)},$$

$$\dot{\varepsilon}_{yy} = -\frac{\partial v}{\partial y} = \dot{\lambda}\frac{\partial f}{\partial \sigma_{yy}} = \sum_{j=1}^{J}\dot{\lambda}_j\frac{\partial f_j}{\partial \sigma_{yy}} = \sum_{j=1}^{J}\dot{\lambda}_j A_{yy}^{(j)},$$

$$\dot{\gamma}_{xy} = -\left(\frac{\partial v}{\partial x} + \frac{\partial u}{\partial y}\right) = \dot{\lambda}\frac{\partial f}{\partial \sigma_{xy}} = \sum_{j=1}^{J}\dot{\lambda}_j\frac{\partial f_j}{\partial \sigma_{xy}} = 2\sum_{j=1}^{J}\dot{\lambda}_j A_{xy}^{(j)}, \tag{5}$$

where $\dot{\lambda}_j$ is the non-negative plastic multiplier associated with the j-th plane of the failure surface. Differentiating eqns (1) with respect to the coordinates and substituting into (5), the flow rule constraints for each triangle may be written as

$$\sum_{i=1}^{3}\frac{\partial N_i}{\partial x}u_i+\sum_{j=1}^{J}\dot{\lambda}_j A_{xx}^{(j)}=0,\quad \sum_{i=1}^{3}\frac{\partial N_i}{\partial y}v_i+\sum_{j=1}^{J}\dot{\lambda}_j A_{yy}^{(j)}=0,\quad \sum_{i=1}^{3}\frac{\partial N_i}{\partial x}v_i+\sum_{i=1}^{3}\frac{\partial N_i}{\partial y}u_i+2\sum_{j=1}^{J}\dot{\lambda}_j A_{xy}^{(j)}=0,$$

where $\dot{\lambda}_j \geqslant 0$ ($j=1,\ldots,J$). By using the shape functions given in (A1), the matrix form of these flow rule constraints, which must be satisfied by every triangle in the mesh, is given by

$$\boldsymbol{A}_{p1}^{e}\boldsymbol{x}_1^{e}-\boldsymbol{A}_{p2}^{e}\boldsymbol{x}_2^{e}=0 \tag{6}$$

where

$$\boldsymbol{A}_{p1}^{e}=\frac{1}{2A}\begin{pmatrix} y_{23} & 0 & y_{31} & 0 & y_{12} & 0\\ 0 & x_{32} & 0 & x_{13} & 0 & x_{21}\\ x_{32} & y_{23} & x_{13} & y_{31} & x_{21} & y_{12}\end{pmatrix},\quad \boldsymbol{x}_1^{e}=\begin{bmatrix} u_1\\ v_1\\ u_2\\ v_2\\ u_3\\ v_3\end{bmatrix},$$

$$\boldsymbol{A}_{p2}^{e}=\begin{pmatrix} A_{xx}^{(1)} & \ldots & A_{xx}^{(j)} & \ldots & A_{xx}^{(J)}\\ A_{yy}^{(1)} & \ldots & A_{yy}^{(j)} & \ldots & A_{yy}^{(J)}\\ 2A_{xy}^{(1)} & \ldots & 2A_{xy}^{(j)} & \ldots & 2A_{xy}^{(J)}\end{pmatrix},\quad \boldsymbol{x}_2^{e}=\begin{bmatrix} \dot{\lambda}_1^{(e)}\\ \vdots\\ \dot{\lambda}_j^{(e)}\\ \vdots\\ \dot{\lambda}_J^{(e)}\end{bmatrix}.$$

The superscript e denotes the element e in the mesh and there are J inequality constraints on the plastic multipliers of the form $\boldsymbol{x}_2^{e}\geqslant 0$.

3.2. Constraints for velocity discontinuities

If the discontinuity is inclined to the x-axis by an angle θ, then a coordinate transformation is required. Let

$$\begin{pmatrix} s\\ t\end{pmatrix}=\begin{bmatrix} \cos\theta & \sin\theta\\ -\sin\theta & \cos\theta\end{bmatrix}\begin{pmatrix} x\\ y\end{pmatrix}. \tag{7}$$

then

$$\begin{pmatrix} v_s\\ v_t\end{pmatrix}=\begin{bmatrix} \cos\theta & \sin\theta\\ -\sin\theta & \cos\theta\end{bmatrix}\begin{pmatrix} u\\ v\end{pmatrix} \tag{8}$$

Hence, the discontinuous constraint eqution (C5) presented in Appendix C can be rewritten as

$$-\sin\theta\Delta u+\cos\theta\Delta v=-(\dot{\kappa}_1+\dot{\kappa}_2)\tan\phi,$$

$$\cos\theta\Delta u+\sin\theta\Delta v=-(\dot{\kappa}_1-\dot{\kappa}_2). \tag{9}$$

where Δu and Δv are velocity jumps in the x- and y-directions, respectively. These jumps are illustrated in Fig. 4.

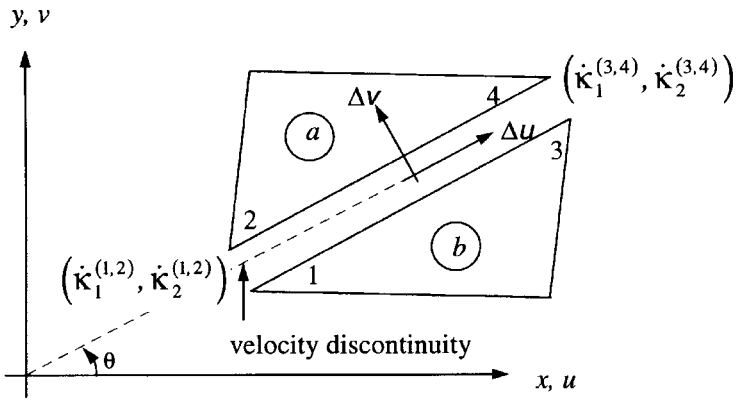

Fig. 4. Velocity discontinuity.

For each discontinuity, therefore, the matrix form of these discontinuity constraints is given by four equations with four unknowns, i.e.

$$\boldsymbol{A}^k_{d1}\boldsymbol{x}^k_1 - \boldsymbol{A}^k_{d3}\boldsymbol{x}^k_3 = 0, \tag{10}$$

where

$$\boldsymbol{A}^k_{d1} = \begin{bmatrix} -\sin\theta & \cos\theta & \sin\theta & -\cos\theta & 0 & 0 & 0 & 0 \\ \cos\theta & \sin\theta & -\cos\theta & -\sin\theta & 0 & 0 & 0 & 0 \\ 0 & 0 & 0 & 0 & -\sin\theta & \cos\theta & \sin\theta & -\cos\theta \\ 0 & 0 & 0 & 0 & \cos\theta & \sin\theta & -\cos\theta & -\sin\theta \end{bmatrix},$$

$$\boldsymbol{A}^k_{d3} = \begin{bmatrix} \tan\phi & \tan\phi & 0 & 0 \\ 1 & -1 & 0 & 0 \\ 0 & 0 & \tan\phi & \tan\phi \\ 0 & 0 & 1 & -1 \end{bmatrix},$$

$$\boldsymbol{x}^k_1 = \begin{pmatrix} u_1 & v_1 & u_2 & v_2 & u_3 & v_3 & u_4 & v_4 \end{pmatrix}^{\mathrm{T}},$$

$$\boldsymbol{x}^k_3 = \begin{pmatrix} \dot{\kappa}_1^{(1,2)^k} & \dot{\kappa}_2^{(1,2)^k} & \dot{\kappa}_1^{(3,4)^k} & \dot{\kappa}_2^{(3,4)^k} \end{pmatrix}^{\mathrm{T}} \geqslant 0,$$

and the superscript k is the index of the discontinuity.

3.3. Constraints for velocity boundary conditions

To be kinematically admissible, the computed velocity field must satisfy the prescribed boundary conditions. Consider a segment of the boundary with the end nodes i_1 and i_2. If the segment is inclined at an angle θ to the x-axis, then by using the coordinate transformation (8) it is found that

$$\begin{bmatrix} \cos\theta & \sin\theta \\ -\sin\theta & \cos\theta \end{bmatrix}\begin{pmatrix} u_i \\ v_i \end{pmatrix} = \begin{pmatrix} \bar{u} \\ \bar{v} \end{pmatrix}$$

where $\bar{u}$ and $\bar{v}$ are prescribed nodal tangential and normal velocity components, respectively and node i denotes a point on the straight line $i_1 i_2$. Thus, these constraints may be expressed in the following matrix form:

$$\boldsymbol{A}_b^i \boldsymbol{x}_1^i = \boldsymbol{b}^i, \tag{11}$$

where

$$\boldsymbol{A}_b^i = \begin{bmatrix} \cos\theta & \sin\theta \\ -\sin\theta & \cos\theta \end{bmatrix}, \quad \boldsymbol{x}_1^i = \begin{pmatrix} u_i \\ v_i \end{pmatrix}, \quad \boldsymbol{b}^i = \begin{pmatrix} \bar{u} \\ \bar{v} \end{pmatrix}.$$

3.4. Objective function

Plastic flow may occur in both the continuum and the velocity discontinuities. The total power dissipated by these means constitutes the objective function, which can be expressed as a function of plastic multipliers and the velocity discontinuity multipliers.

3.5. Power dissipation in a plastic region

Within each triangle, the power dissipated by the plastic stresses is given by

$$P_c^e = \int_{A^e} \left(\sigma_{xx}\dot{\varepsilon}_{xx} + \sigma_{yy}\dot{\varepsilon}_{yy} + \sigma_{xy}\dot{\gamma}_{xy}\right) \mathrm{d}A = \sum_{j=1}^{J} \dot{\gamma}_j \int_{A^e} G^{(j)} \, \mathrm{d}A,$$

where A^e denote the area of the triangle and $G^{(j)}$ are defined in Appendix B. Therefore, the power dissipated by the plastic stresses may be evaluated by

$$P_c^e = \left(\boldsymbol{c}_c^e\right)^{\mathrm{T}} \boldsymbol{x}_2^e \tag{12}$$

where

$$\boldsymbol{c}_c^e = \begin{bmatrix} \int_{A^e} G^{(1)} \, \mathrm{d}A \\ \int_{A^e} G^{(2)} \, \mathrm{d}A \\ \vdots \\ \int_{A^e} G^{(J)} \, \mathrm{d}A \end{bmatrix}, \quad \boldsymbol{x}_2^e = \begin{bmatrix} \dot{\gamma}_1^{(e)} \\ \dot{\gamma}_2^{(e)} \\ \vdots \\ \dot{\gamma}_J^{(e)} \end{bmatrix}$$

and $\boldsymbol{x}_2^e \geqslant 0$.

3.6. Power dissipation along a velocity discontinuity

From the discussion in Appendix C, the power dissipated by plastic shearing along each velocity discontinuity k is given by an integral of the form

$$P_d^k = \int_l c(\dot{\kappa}_1 + \dot{\kappa}_2)\,\mathrm{d}l$$

where l denotes the length of the discontinuity and c is the cohesion of the matrix material. Therefore, the power dissipated by the discontinuity may be evaluated by:

$$P_d^k = \left(\boldsymbol{c}_d^k\right)^{\mathrm{T}} \boldsymbol{x}_3^k \tag{13}$$

where

$$\boldsymbol{c}_d^k = \frac{1}{2}\begin{bmatrix} \int_l c\,\mathrm{d}l \\ \int_l c\,\mathrm{d}l \\ \int_l c\,\mathrm{d}l \\ \int_l c\,\mathrm{d}l \end{bmatrix}, \quad \boldsymbol{x}_3^k = \begin{bmatrix} \dot{\kappa}_1^{(1,2)^k} \\ \dot{\kappa}_2^{(1,2)^k} \\ \dot{\kappa}_1^{(3,4)^k} \\ \dot{\kappa}_2^{(3,4)^k} \end{bmatrix}.$$

3.7. External work due to the weight of soil

The external work expended in displacing the weight of soil within an element e is given by

$$W_\gamma^e = \int_{A^e} \left(\gamma_x u + \gamma_y \upsilon\right)\,\mathrm{d}A = \frac{1}{3}\gamma_x A^e(u_1 + u_2 + u_3) + \frac{1}{3}\gamma_y A^e(\upsilon_1 + \upsilon_2 + \upsilon_3)$$

where γ_x and γ_y are components of the unit weight of the deposit in the x- and y-directions, respectively, and where u_i, υ_i $(i = 1, 2, 3)$ are velocity components at the nodal points of the element, and A^e denotes the area of this element, viz

$$W_\gamma^e = \left(\boldsymbol{c}_\gamma^e\right)^T \boldsymbol{x}_1^e \tag{14}$$

where

$$\boldsymbol{c}_\gamma^e = \frac{A^e}{3}\begin{bmatrix} \gamma_x \\ \gamma_y \\ \gamma_x \\ \gamma_y \\ \gamma_x \\ \gamma_y \end{bmatrix}, \quad \boldsymbol{x}_1^e = \begin{bmatrix} u_1 \\ \upsilon_1 \\ u_2 \\ \upsilon_2 \\ u_3 \\ \upsilon_3 \end{bmatrix}.$$

Equating the external work to the power dissipated provides the quantity Q to be minimised by an appropriate optimisation programme. Therefore, the linear programming problem corresponding to the upper bound is defined by

$$\text{Minimise} \quad Q = P_c + P_d - W\gamma$$

$$\begin{array}{lll} \text{Subject to} & \boldsymbol{A}_{p1}\boldsymbol{x}_1 - \boldsymbol{A}_{p2}\boldsymbol{x}_2 & = 0 \\ & \boldsymbol{A}_{d1}\boldsymbol{x}_1 \quad -\boldsymbol{A}_{d3}\boldsymbol{x}_3 & = 0 \\ & \boldsymbol{A}_b\boldsymbol{x}_1 & = \boldsymbol{b} \\ & \boldsymbol{x}_2 \geqslant 0 & \\ & \boldsymbol{x}_3 \geqslant 0 & \end{array}$$

where

$$P_c = \sum_{e=1}^{E} P_c^e$$

$$P_d = \sum_{k=1}^{D} P_d^k$$

$$W_\gamma = \sum_{e=1}^{E} W_\gamma^e$$

$$\boldsymbol{A}_{p1} = \sum_{e=1}^{E} \boldsymbol{A}_{p1}^e$$

$$\boldsymbol{A}_{p2} = \sum_{e=1}^{E} \boldsymbol{A}_{p2}^e$$

$$\boldsymbol{A}_{d1} = \sum_{k=1}^{D} \boldsymbol{A}_{d1}^k$$

$$\boldsymbol{A}_{d3} = \sum_{k=1}^{D} \boldsymbol{A}_{d3}^k$$

$$\boldsymbol{A}_b = \sum_{i=1}^{I} \boldsymbol{A}_b^i$$

$$\boldsymbol{b} = \sum_{i=1}^{I} \boldsymbol{b}^i$$

and

$$\boldsymbol{x}_1 = \begin{bmatrix} u_1 \\ v_1 \\ u_2 \\ v_2 \\ \vdots \\ u_N \\ v_N \end{bmatrix}, \quad \boldsymbol{x}_2 = \begin{bmatrix} \dot{\lambda}_1^{(1)} \\ \dot{\lambda}_2^{(1)} \\ \vdots \\ \dot{\lambda}_J^{(1)} \\ \vdots \\ \dot{\lambda}_1^{(E)} \\ \dot{\lambda}_2^{(E)} \\ \vdots \\ \dot{\lambda}_J^{(E)} \end{bmatrix}, \quad \boldsymbol{x}_3 = \begin{bmatrix} \dot{\kappa}_1^{(1,2)^1} \\ \dot{\kappa}_2^{(1,2)^1} \\ \dot{\kappa}_1^{(3,4)^1} \\ \dot{\kappa}_2^{(3,4)^1} \\ \vdots \\ \dot{\kappa}_1^{(1,2)^D} \\ \dot{\kappa}_2^{(1,2)^D} \\ \dot{\kappa}_1^{(3,4)^D} \\ \dot{\kappa}_2^{(3,4)^D} \end{bmatrix}$$

E is the number of elements, D is the number of discontinuities, N is the number of nodes and I is the number of segments along the boundary.

4. Formulation of the lower bound problem

The lower bound theorem of the classical plasticity theory considers only equilibrium and failure and gives no consideration to kinematics. It is a powerful tool for analysing the stability of problems in soil mechanics. The theory assumes a perfectly plastic soil model with an associated flow rule and states that any statically admissible stress field will furnish a lower bound estimate of the true limit load. The conditions required to establish a lower bound solution to the collapse load are essentially as follows:

> The loads, determined from a distribution of stress alone, that satisfy (a) the equilibrium equations, (b) the stress boundary conditions and (c) nowhere violates the yield criterion, are not greater than the actual collapse load.

Similar to the formulation of the upper bound problem, the formulation of the lower bound problem also permits discontinuities in the stress field. In the present formulation, triangular elements are used to model the stress field under conditions of plane strain (Fig. 2). The constraints in the problem will be imposed on the stresses by the equilibrium equations, the stress boundary conditions, the discontinuity equilibrium equations and the failure functions.

Assume that the variation of the stress throughout each element is linear and each node is associated with three stress components (shown in Fig. 5) which can be expressed as:

$$\begin{aligned} \sigma_{xx} &= \sum_{i=1}^{3} N_i \sigma_{xx}^i, \\ \sigma_{yy} &= \sum_{i=1}^{3} N_i \sigma_{yy}^i, \\ \sigma_{xy} &= \sum_{i=1}^{3} N_i \sigma_{xy}^i, \end{aligned} \tag{15}$$

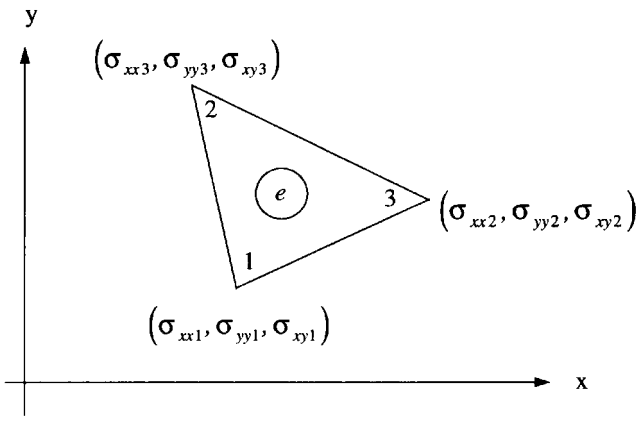

Fig. 5. Triangular element for lower bound limit analysis.

where σ^i_{xx}, σ^i_{yy}, σ^i_{xy} $(i = 1, 2, 3)$ are nodal stress components and N_i are linear shape functions (A1).

4.1. Constraints for element equilibrium

In order to satisfy equilibrium, the stresses throughout each triangular element must obey the stress equilibrium equations:

$$\frac{\partial \sigma_{xx}}{\partial_x} + \frac{\partial \sigma_{xy}}{\partial y} = \gamma_x,$$

$$\frac{\partial \sigma_{xy}}{\partial_x} + \frac{\partial \sigma_{yy}}{\partial y} = \gamma_y. \tag{16}$$

The stress must also satisfy the boundary conditions

$$\boldsymbol{n}\sigma = \boldsymbol{q} \tag{17}$$

where γ_x and γ_y denote the components of body force in the x- and y-directions, respectively, and where $\boldsymbol{n}$ is the outward unit normal vector to a surface element and $\boldsymbol{q}$ is a surface traction vector.

By using the eqn (15) and the shape functions (A1), the discrete equilibrium equations expressed in terms of the nodal stresses have the form of

$$\boldsymbol{A}^e_{\mathrm{eq}}\boldsymbol{x}^e = \boldsymbol{b}^e_{\mathrm{eq}} \tag{18}$$

where

$$\boldsymbol{A}^e_{\mathrm{eq}} = \frac{1}{2A^e}\begin{pmatrix} y_{23} & 0 & x_{32} & y_{31} & 0 & x_{13} & y_{12} & 0 & x_{21} \\ 0 & x_{32} & y_{23} & 0 & x_{13} & y_{31} & 0 & x_{21} & y_{12} \end{pmatrix},$$

$$\boldsymbol{x}^e = \begin{pmatrix} \sigma^e_{xx1} & \sigma^e_{yy1} & \sigma^e_{xy1} & \sigma^e_{xx2} & \sigma^e_{yy2} & \sigma^e_{xy2} & \sigma^e_{xx3} & \sigma^e_{yy3} & \sigma^e_{xy3} \end{pmatrix}^{\mathrm{T}},$$

$$\boldsymbol{b}^e_{\mathrm{eq}} = \begin{pmatrix} \gamma_x \\ \gamma_y \end{pmatrix}$$

and where A^e is the area of the element e.

4.2. Constraints for boundary conditions

Following Sloan (1988), a special boundary condition relevant to many geotechnical engineering problems is used, i.e., the stress boundary condition (17) takes the following values

$$\sigma_n = q = \text{constant},$$

$$\tau = t = \text{constant}.$$

Assuming that the edge i of a triangle e has endpoints 1 and 2, and q_k, t_k ($k = 1, 2$) are the normal stresses and shear stresses specified at the nodes 1 and 2, respectively (shown in Fig. 6). Since each of the stress components σ_{xx}, σ_{yy}, σ_{xy} varies linearly within each element, i.e., they vary linearly along the edge i, then it is possible to cater for a slightly more general type of boundary condition of the form

$$\sigma_n^i = q_1 + (q_2 - q_1)\frac{\eta}{L},$$

$$\tau^i = t_1 + (t_2 - t_1)\frac{\eta}{L},$$

where $\eta \in [0, 1]$ denotes the local coordinate along the edge i. If the edge i is inclined to the x-axis by an angle θ^i, then with reference to Fig. 6, the normal stress and shear stress are given by

$$\begin{pmatrix} \sigma_n^i \\ \tau^i \end{pmatrix} = \begin{pmatrix} \sin^2\theta^i & \cos^2\theta^i & -\sin 2\theta^i \\ -\frac{1}{2}\sin 2\theta^i & \frac{1}{2}\sin 2\theta^i & \cos 2\theta^i \end{pmatrix} \begin{pmatrix} \sigma_{xx}^i \\ \sigma_{yy}^i \\ \sigma_{xy}^i \end{pmatrix}. \tag{19}$$

The stress boundary conditions give rise to the equations

$$\boldsymbol{A}_b^i \boldsymbol{x}^i = \boldsymbol{b}_b^i \tag{20}$$

where

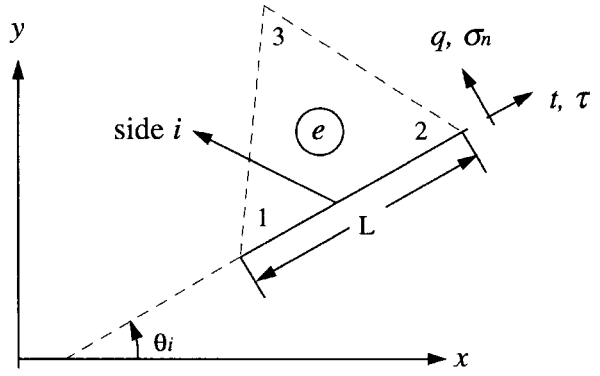

Fig. 6. Stress boundary conditions.

$$\boldsymbol{A}_b^i = \begin{bmatrix} \sin^2\theta^i & \cos^2\theta^i & -\sin 2\theta^i & 0 & 0 & 0 \\ -\frac{1}{2}\sin 2\theta^i & \frac{1}{2}\sin 2\theta^i & \cos 2\theta^i & 0 & 0 & 0 \\ 0 & 0 & 0 & \sin^2\theta^i & \cos^2\theta^i & -\sin 2\theta^i \\ 0 & 0 & 0 & -\frac{1}{2}\sin 2\theta^i & \frac{1}{2}\sin 2\theta^i & \cos 2\theta^i \end{bmatrix},$$

$$\boldsymbol{x}^i = \begin{pmatrix} \sigma^i_{xx1} & \sigma^i_{yy1} & \sigma^i_{xy1} & \sigma^i_{xx2} & \sigma^i_{yy2} & \sigma^i_{xy2} \end{pmatrix}^{\mathrm{T}},$$

$$\boldsymbol{b}_b^i = \begin{pmatrix} q_1 & t_1 & q_2 & t_2 \end{pmatrix}^{\mathrm{T}}.$$

4.3. Stress discontinuity constraints

In order to permit statically admissible discontinuities at the edges of adjacent triangles, it is necessary to enforce additional constraints on the nodal stresses. A statically admissible stress discontinuity permits the normal stress component parallel to the discontinuity to be discontinuous, but requires continuity of the corresponding shear and normal components. Assume that two elements a and b share a side k defined by the nodal pairs (1, 2) and (3, 4), as shown in Fig. 7. If k is a discontinuity, equilibrium at every point along k requires:

$$\sigma_n^a = \sigma_n^b,$$

$$\tau^a = \tau^b$$

where the superscripts a and b are used to denote the elements a and b, respectively.

Noting that the stresses vary linearly along each element edge, the above condition is equivalent to enforcing the constraints

$$\begin{bmatrix} \sigma^a_{n1} \\ \sigma^a_{n3} \\ \tau^a_1 \\ \tau^a_3 \end{bmatrix} = \begin{bmatrix} \sigma^b_{n2} \\ \sigma^b_{n4} \\ \tau^b_2 \\ \tau^b_4 \end{bmatrix}.$$

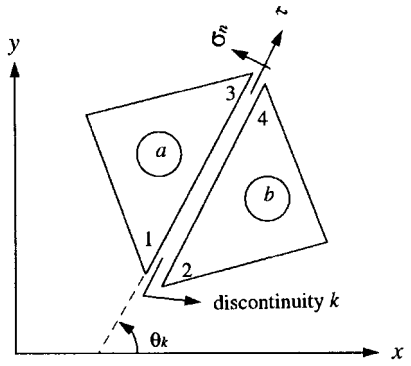

Fig. 7. Statically admissible stress discontinuity between adjacent triangles.

If the discontinuity k is inclined to the x-axis by an angle θ_k then by substituting eqn (19) into the above matrix, the constraints for the discontinuity equilibrium form the following matrix equation:

$$\boldsymbol{A}_d^k \boldsymbol{x}^k = 0 \tag{21}$$

where

$$\boldsymbol{A}_d^k = \begin{pmatrix} T & -T & 0 & 0 \\ 0 & 0 & T & -T \end{pmatrix},$$

$$\boldsymbol{x}^k = \begin{pmatrix} \sigma_{xx1}^a & \sigma_{yy1}^a & \sigma_{xy1}^a & \sigma_{xx2}^b & \sigma_{yy2}^b & \sigma_{xy2}^b & \sigma_{xx3}^a & \sigma_{yy3}^a & \sigma_{xy3}^a & \sigma_{xx4}^b & \sigma_{yy4}^b & \sigma_{xy4}^b \end{pmatrix}^{\mathrm{T}}$$

and where

$$T = \begin{pmatrix} \sin^2\theta^k & \cos^2\theta^k & -\sin 2\theta^k \\ -\frac{1}{2}\sin 2\theta^k & \frac{1}{2}\sin 2\theta^k & \cos 2\theta^k \end{pmatrix}.$$

4.4. Constraints for the failure condition

From the discussion of Appendix B, the linearized failure functions of the material with vertical or horizontal fissures, or both, can be written as follows:

$$A_{xx}^{(j)}\sigma_{xx} + A_{yy}^{(j)}\sigma_{yy} + 2A_{xy}^{(j)}\sigma_{xy} \le G^{(j)}, \quad j = 1, 2, \ldots, J \tag{22}$$

where $A_{xx}^{(j)}$, $A_{yy}^{(j)}$, $A_{xy}^{(j)}$, $j = 1, 2, \ldots, J$, as defined by eqns (B9)–(B11).

Since the failure condition must be satisfied throughout the stress field, it is sufficient to enforce the constraints (22) at each nodal point of each element. Hence, the constraint equations imposed on the stresses at the node n can be given by the matrix equation

$$\boldsymbol{A}_f^n \boldsymbol{x}^n \le \boldsymbol{b}_f^n \tag{23}$$

where

$$\boldsymbol{A}_f^n = \begin{bmatrix} A_{xx}^{(1)} & A_{yy}^{(1)} & 2A_{xy}^{(1)} \\ A_{xx}^{(2)} & A_{yy}^{(2)} & 2A_{xy}^{(2)} \\ \vdots & \vdots & \vdots \\ A_{xx}^{(J)} & A_{yy}^{(J)} & 2A_{xy}^{(J)} \end{bmatrix}, \quad \boldsymbol{x}^n = \begin{pmatrix} \sigma_{xxn} \\ \sigma_{yyn} \\ \sigma_{xyn} \end{pmatrix}, \quad \boldsymbol{b}_f^n = \begin{bmatrix} G^{(1)} \\ G^{(2)} \\ \vdots \\ G^{(J)} \end{bmatrix}.$$

4.5. Objective functions

According to the lower bound theorem, the stress components σ_{xx}, σ_{yy}, σ_{xy} must be in equilibrium with the external loads q_i and the influence of the gravity acting on the material. By assuming unit thickness out-of-plane, the collapse load is defined by

$$Q = \int_l \sigma_n \, \mathrm{d}l + \int_A \gamma \, \mathrm{d}A = Q_1 + Q_2$$

where l is the length of the loading boundary, σ_n is the normal stress acting over the boundary and A is the area considered. The above equation is derived under the assumption of unit thickness in the out-of-plane direction.

It is obvious that $Q_2 = \int_A \gamma \, \mathrm{d}A$ is a constant for many geotechnical problems, so the objective function can be defined by $Q = \int_l \sigma_n \, \mathrm{d}l = Q_1$. Since the stresses vary linearly throughout each element, then along each segment i on the loading boundary $Q^i = (L/2)\,(\sigma_{n1} + \sigma_{n2})$ where L is the length of the edge i and σ_{n1}, σ_{n2} are the normal stresses at the nodes 1 and 2 (Fig. 6). If θ_i denotes the inclination of the edge i to the x-axis, then by using eqn (19) it follows that

$$Q^i = (\boldsymbol{c}^i)^{\mathrm{T}} \boldsymbol{x}^i \tag{24}$$

where

$$\boldsymbol{c}^i = \frac{L}{2} \begin{bmatrix} \sin^2 \theta_i \\ \cos^2 \theta_i \\ -\sin 2\theta_i \\ \sin^2 \theta_i \\ \cos^2 \theta_i \\ -\sin 2\theta_i \end{bmatrix}, \quad \boldsymbol{x}^i = \begin{bmatrix} \sigma^i_{xx1} \\ \sigma^i_{yy1} \\ \sigma^i_{xy1} \\ \sigma^i_{xx2} \\ \sigma^i_{yy2} \\ \sigma^i_{xy2} \end{bmatrix}.$$

4.6. Linear programming problem

Combining all the constraint eqns (18), (20), (21), (23) and (24), the linear programming problem corresponding to the lower bound can be defined as follows:

$$\text{Maximise} \quad \boldsymbol{c}^{\mathrm{T}} \boldsymbol{x},$$

$$\text{Subject to} \quad \boldsymbol{A}_1 \boldsymbol{x} = \boldsymbol{b}_1, \quad \boldsymbol{A}_2 \boldsymbol{x} \leqslant \boldsymbol{b}_2,$$

where

$$\boldsymbol{c} = \sum_{i=1}^{I_1} \boldsymbol{c}^i,$$

$$\boldsymbol{A}_1 = \sum_{e=1}^{E} \boldsymbol{A}^e_{\mathrm{eq}} + \sum_{k=1}^{D} \boldsymbol{A}^k_d + \sum_{i=1}^{I^2} \boldsymbol{A}^i_b,$$

$$\boldsymbol{A}_2 = \sum_{n=1}^{N} \boldsymbol{A}^n_f,$$

$$\boldsymbol{x} = \left(\sigma_{xx1} \quad \sigma_{yy1} \quad \sigma_{xy1} \quad \sigma_{xx2} \quad \sigma_{yy2} \quad \sigma_{xy2} \quad \ldots \quad \sigma_{xxN} \quad \sigma_{yyN} \quad \sigma_{xyN}\right)^{\mathrm{T}},$$

$$\boldsymbol{b}_1 = \sum_{e=1}^{E} \boldsymbol{b}_{\mathrm{eq}}^{e} + \sum_{i=1}^{I_2} \boldsymbol{b}_{b}^{i},$$

$$\boldsymbol{b}_2 = \sum_{n=1}^{N} \boldsymbol{b}_{f}^{n}.$$

N is the number of nodes, E is the number of elements, D is the number of discontinuous edges, I_1 is the number of segments along the loading boundary and I_2 is the number of segments along the boundary with prescribed tractions.

5. Applications

In order to validate the present formulation for fissured materials, several examples are solved in this section. The techniques described above are used to predict the collapse load for a rigid strip footing. Since the exact collapse load for a weightless material is known (Zheng and Booker, 1997), it provides a useful check on the ability of the new methods to provide accurate upper and lower bounds. To ascertain the suitability of the new formulations for more general cases, such as the bearing capacity problems of rough or smooth footings on materials with or without unit weight, additional examples are presented. Also, the results of investigations to ascertain the sensitivity of the new formulations to the mesh refinement and the failure surface approximation will be given.

5.1. Bearing capacity of a weightless material

The exact collapse pressure q_F for a smooth or rough rigid strip footing on the surface of a weightless fissured deposit may be expressed simply as $q_F = cN_c$, where expressions for the bearing capacity factor N_c for vertically and horizontally fissured materials are given by Zheng and Booker (1997). These exact solutions will be compared with the predictions obtained using the upper and lower bound techniques described above.

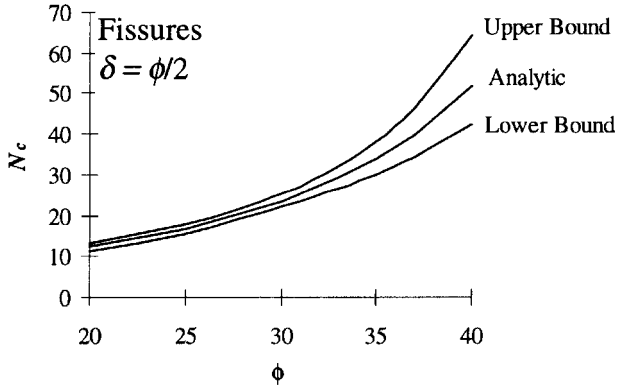

Fig. 8. Bearing capacity of a rigid strip footing on a vertically fissured deposit ($\delta = \phi/2$).

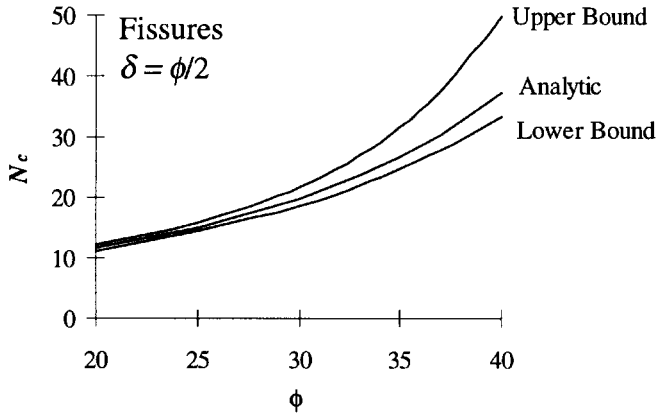

Fig. 9. Bearing capacity of a rigid strip footing on a vertically and horizontally fissured deposit ($\delta = \phi/2$).

To investigate the sensitivity of the predicted bounds to the numerical procedure, two different meshes, one coarse and one fine, have been used to estimate the upper and lower bounds. Different approximations of the failure surfaces, involving a different number of planes in the linearized failure surfaces, J, were also used to calculate upper and lower bounds.

The results plotted in Figs. 8 and 9 indicate the variation of the bearing capacity factor N_c with the angle of internal friction of the material matrix, ϕ, for the range $20^\circ \leqslant \phi \leqslant 40^\circ$, and with the angle of friction on the fissures $\delta = \phi/2$. The strength of the fissures is purely frictional. Fig. 8 shows the results for a weightless vertically fissured material and Fig. 9 presents the results for a weightless material with both vertical and horizontal fissures. These figures show that the computed bounds are strict upper and lower bounds of the exact failure loads.

To investigate the influences of the mesh and the approximate failure surface, the problem of a rough or smooth rigid footing on a vertically fissured material with the friction angles $\phi = 30^\circ$ and $\delta = \phi/2$ is examined. The results in Table 1 are the upper bounds obtained by using a coarse mesh (Fig. 10, Mesh 1) and a fine mesh (Fig. 11, Mesh 2) for selected values of J (number of planes in the linearised failure surface). The results in Table 2 are the lower bounds obtained by using a coarse mesh (Fig. 12, Mesh 3) and a fine mesh (Fig. 13, Mesh 4) for selected values of J.

The results in Figs. 8 and 9 establish that the upper and lower bounds are reasonably accurate, as the analytic solutions are bracketed closely by the numerical bound solutions. It is obvious from the results in Tables 1 and 2, that by refining the mesh or by using a more accurate approximation to the failure surface, the accuracy in both upper and lower bounds is improved.

Table 1
Upper bound results of a vertically fissured deposit with $\phi = 30^\circ$ and $\delta = \phi/2$

Mesh	J	N_c	N_c error (%)
Mesh 1	12	27.575	17.377
Mesh 2	12	25.670	9.269
Mesh 1	24	27.257	16.024
Mesh 2	24	25.116	6.910
Mesh 1	96	27.234	15.926
Mesh 2	96	25.064	6.689

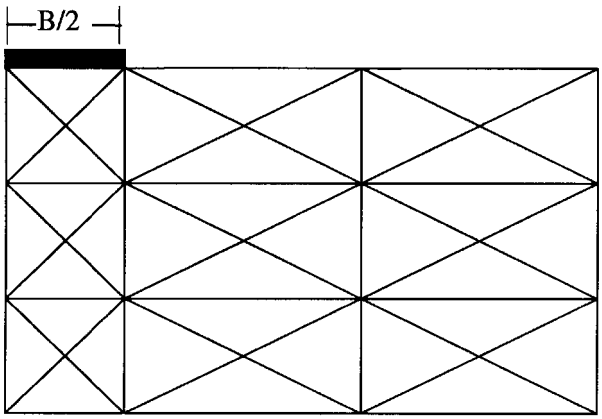

Fig. 10. Mesh 1 for upper bound analysis of a rigid strip footing.

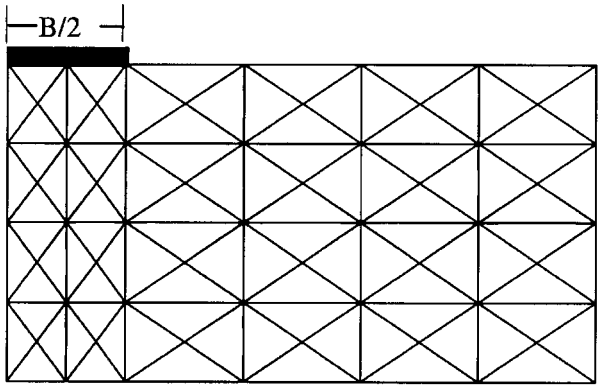

Fig. 11. Mesh 2 for upper bound analysis of a rigid strip footing.

Table 2
Lower bound results of a vertically fissured deposit with $\phi = 30^\circ$ and $\delta = \phi/2$

Mesh	J	N_c	N_c error (%)
Mesh 3	12	21.951	17.377
Mesh 4	12	22.030	9.269
Mesh 3	24	21.968	16.024
Mesh 4	24	22.037	6.196
Mesh 3	96	22.110	5.885
Mesh 4	96	22.132	5.791

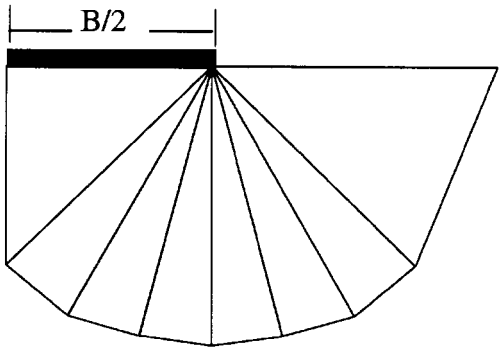

Fig. 12. Mesh 3 for lower bound analysis of a rigid strip footing.

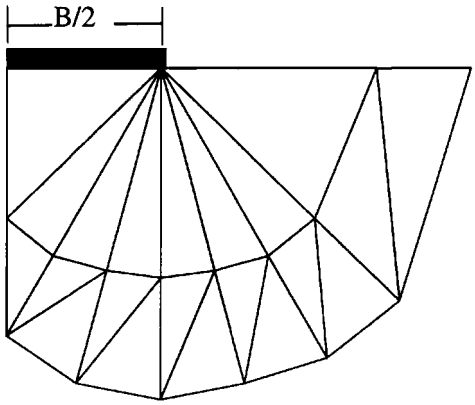

Fig. 13. Mesh 4 for lower bound analysis of a rigid strip footing.

Table 3
Bearing capacity of smooth footing with unit weight, $\gamma B/c = 1$

Material	Lower bound	Characteristics solution	Upper bound
Vertically fissured	27.667	29.7061	34.364
Horizontally fissured	27.977	30.2354	35.584
Vertically and horizontally fissured	22.615	24.7845	29.263

Table 4
Bearing capacity of smooth footing without unit weight, $\gamma B/c = 0$

Material	Lower bound	Characteristics solution	Upper bound
Vertically fissured	22.138	22.6635	25.116
Horizontally fissured	22.132	22.6635	25.602
Vertically and horizontally fissured	18.724	19.0666	21.711

Table 5
Bearing capacity of rough footing with unit weight, $\gamma B/c = 1$

Material	Lower bound	Characteristics solution	Upper bound
Vertically fissured	33.415	34.5294	44.975
Horizontally fissured	32.657	36.5480	44.996
Vertically and horizontally fissured	25.992	28.7688	36.471

Table 6
Bearing capacity of rough footing without unit weight, $\gamma B/c = 0$

Material	Lower bound	Characteristics solution	Upper bound
Vertically fissured	22.752	23.4323	28.965
Horizontally fissured	22.716	23.4323	28.903
Vertically and horizontally fissured	19.055	19.7589	21.711

5.2. Bearing capacity of a smooth footing on a fissured material

Consider a smooth strip rigid footing resting on the surface of a fissured material with the angles of friction $\phi = 30^\circ$ and $\delta = \phi/2$. Tables 3 and 4 give the bearing capacity of the smooth footing on the fissured materials with unit weight ($\gamma \neq 0$) and without unit weight ($\gamma = 0$), respectively. In these tables, solutions obtained independently using the method of characteristics are also presented. The upper and lower bound solutions were computed using Mesh 2 (Fig. 11) and Mesh 4 (Fig. 13), respectively. In both cases, $J = 96$.

Tables 3 and 4 show that the lower bounds are generally much more accurate than the upper bounds. The bound results for the material with unit weight are generally less accurate than the results for the weightless material, when each is compared with the appropriate results obtained by the method of characteristics. The results also show that for the material with unit weight, the calculated upper bounds overestimate the true capacity by approximately 18% and the lower bounds underestimate the true capacity by approximately 9%.

5.3. Bearing capacity of a rough footing on a fissured material

Consider a rough strip rigid footing resting on the surface of a fissured material with the angles of friction $\phi = 30^\circ$ and $\delta = \phi/2$. Tables 5 and 6 give the bearing capacity of the rough footing on the fissured materials with unit weight and without unit weight, respectively. Solutions obtained independently using the method of characteristics are also shown in these tables. The upper and lower bound solutions were computed using Mesh 2 (Fig. 11) and Mesh 4 (Fig. 13), respectively. In both cases, $J = 96$.

Tables 5 and 6 show that, as in the case of the smooth footings, the lower bounds are generally much more accurate than the upper bounds. The results for the material with unit weight are less accurate than the results for the weightless material when each is compared with the appropriate results obtained by the method of characteristics. The results also show that, for the material with unit weight, the upper bounds overestimate the true capacity by approximately 30% and the lower bounds underestimate the

true capacity by approximately 11%. As indicated previously, the level of accuracy can be improved by selecting a finer mesh and a large number of linear segments to approximate the failure surface.

6. Conclusion

Formulations for the upper bound and lower bound limit analysis of fissured materials have been presented. The numerical results indicate that both upper and lower bound methods are sufficiently accurate for practically calculations, and may be used in tandem with each other to provide useful bounds on the exact collapse load. For weightless fissured materials, Table 1 shows that the error in the upper bound is of the order of 7% for the fine upper bound mesh and $J = 96$. Table 2 shows that the error in the lower bound is also of the order of 7% for the fine lower bound mesh and $J = 96$. Tables 1 and 2 indicate generally, that by increasing the number of planes in the failure surface or refining the meshes, the accuracy of the solutions will be raised. The results in Tables 3–6 for the cohesive-frictional material with unit weight indicate that, although the collapse predictions obtained using the given mesh and linearised failure functions are less accurate than those for the weightless materials, they are still sufficiently precise for practical applications. Hence, the upper bound and the lower bound methods presented in this paper are considered to be useful practical methods for analysing the bearing capacity of fissured materials.

Acknowledgements

The work described in this paper was supported by a research grant awarded by the Australian Research Council. The authors would like to thank Prof. S.W. Sloan for making available the upper and lower bound codes used as the basis for calculating the numerical results presented in this paper.

Appendix A: shape functions

In order to formulate the upper and lower bound problems as linear programming problems, it is necessary to use linear shape functions to approximate the non-linear field quantities in the problem. To achieve this, assume that the considered region is modelled by the triangular elements under conditions

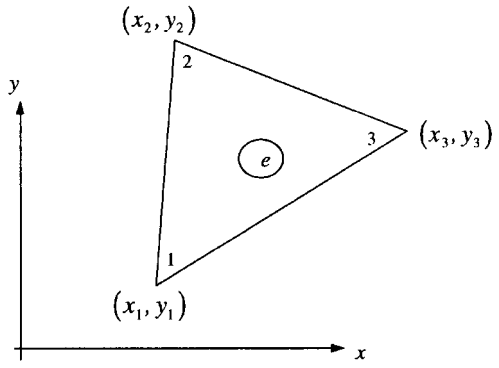

Fig. A1. Traingular element used in limit analysis.

of plane strain and the coordinates of the three vertices of a triangle are given by (x_1, y_1), (x_2, y_2) and (x_3, y_3), as shown in Fig. A1. The linear shape functions can then be defined as follows:

$$N_1 = \frac{1}{2A}\{(x_2y_3 - x_3y_2) + y_{23}x + x_{32}y\},$$

$$N_2 = \frac{1}{2A}\{(x_3y_1 - x_1y_3) + y_{31}x + x_{13}y\},$$

$$N_3 = \frac{1}{2A}\{(x_1y_2 - x_2y_1) + y_{12}x + x_{21}y\}, \tag{A1}$$

where

$$x_{32} = x_3 - x_2, \quad y_{23} = y_2 - y_3,$$

$$x_{13} = x_1 - x_3, \quad y_{23} = y_2 - y_3,$$

$$x_{21} = x_2 - x_1, \quad y_{12} = y_1 - y_2,$$

and

$$A = \frac{1}{2}|x_{13}y_{23} - x_{32}y_{31}|$$

is the element area.

Appendix B: failure surface

Failure

A typical deposit of fissured material is shown schematically in Fig. 1. It consists of two sets of parallel and equally spaced fissures separating blocks of the matrix material. For conditions of plane strain in the x–y plane, failure of a perfectly plastic material is usually written in the form:

$$f(\sigma_{xx}, \sigma_{yy}, \sigma_{xy}) = 0 \tag{B1}$$

where $\sigma_{xx}, \sigma_{yy}, \sigma_{xy}$ denote the Cartesian stress components and where the usual geomechanics convention of regarding compressive stresses as positive is adopted.

It is convenient to introduce an alternative set of variables:

$$X = \frac{1}{2}(\sigma_{xx} - \sigma_{yy}) = R\cos 2\Omega$$

$$Y = \sigma_{xy} = R\sin 2\Omega$$

$$p = \frac{1}{2}(\sigma_{xx} + \sigma_{yy}) \tag{B2}$$

where it will be recognised that p is the mean stress, R is the radius of the Mohr circle and Ω is the angle between the major principal stress direction and the x-axis.

The fissure–matrix composite may fail by either the development of plastic failure in the matrix blocks or by shear failure along the fissures. The failure surface for a geo-material weakened by a single set of fissures, can be defined by (Zheng and Booker, 1997)

$$F(p, \Omega, R) = f_0 f_1 f_2 = 0 \tag{B3}$$

where

$$f_0 = R - \sin\phi(p + q),$$

$$f_1 = R - \frac{\sin\delta(p + q_f)}{\sin(2\Omega - 2\xi + \delta)},$$

$$f_2 = R + \frac{\sin\delta(p + q_f)}{\sin(2\Omega - 2\xi + \delta)}, \tag{B4}$$

where

$$q = c\cot\phi,$$

$$q_f = c_f\cot\delta,$$

and where c and c_f are the cohesion of the matrix and the fissures, respectively. ϕ is the angle of internal friction of the matrix and δ is the angle of friction on the fissures. Attention is restricted to materials for which $\delta \leqslant \phi$ and $q_f \leqslant q$.

Clearly, failure on the fissures is represented by a pair of planes, and failure in the fissure–matrix composite can occur either through failure in the matrix or failure on the fissures. Thus, the failure condition will be bounded by both the cone shown in Fig. B1 (corresponding to failure in the matrix)

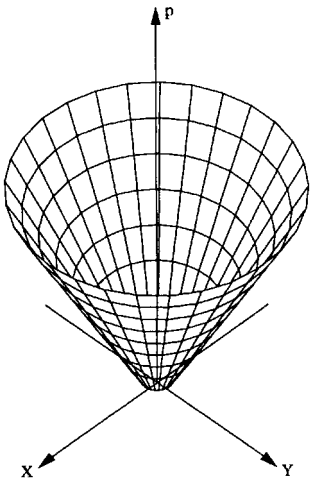

Fig. B1. Failure surface in the matrix.

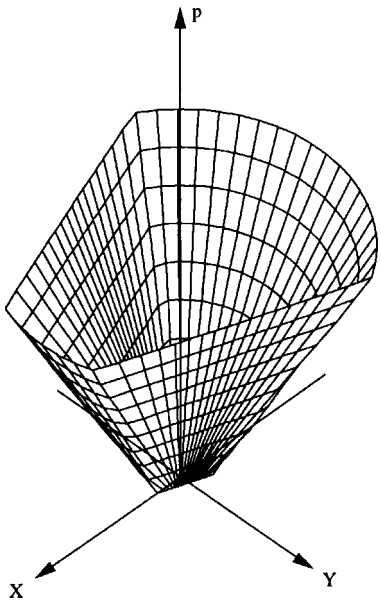

Fig. B2. Composite failure surface in X, Y, p stress space ($\xi = 0$).

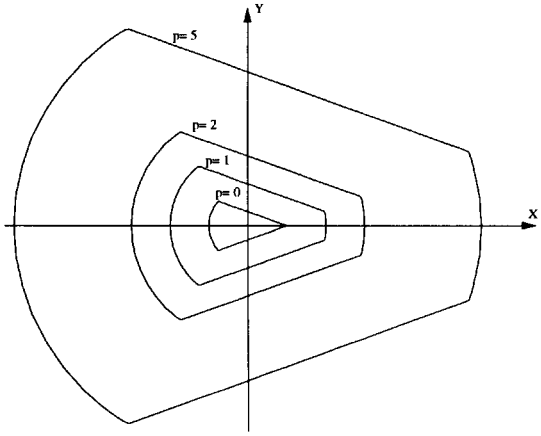

Fig. B3. Contours of the composite failure surface in X, Y stress space ($\xi = 0$).

and by the pair of planes given by f_1 and f_2 in eqn (B4). This leads to the composite failure surface shown in Fig. B2 in X, Y, p stress space, and Fig. B3 which shows a section in the X, Y stress space.

Similarly, if a geo-material is weakened by two sets of fissures, its failure surface is defined by

$$f(p, \Omega, R) = f_0 f_1 f_2 f_3 f_4 = 0 \tag{B5}$$

where f_0, f_1, f_2 are given in eqn (B4) and f_3, f_4 are defined by

$$f_3 = R + \frac{\sin \delta(p + q_f)}{\sin (2\Omega - 2\xi + \delta)},$$

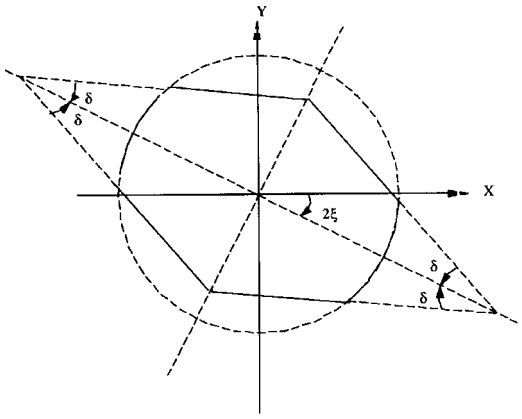

Fig. B4. Failure surface for a material with two sets of fissures and $\alpha \leqslant \pi/2 - \delta$.

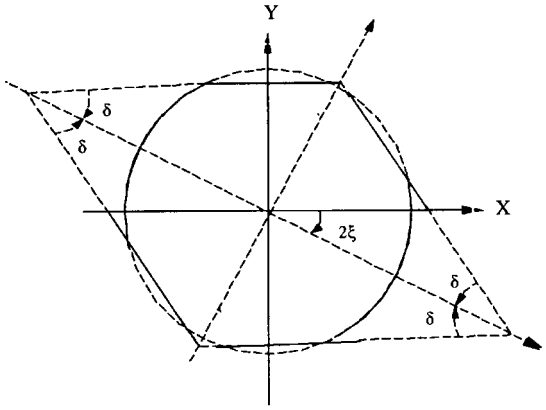

Fig. B5. Failure surface for a material with two sets of fissures and $\alpha \geqslant \pi/2 - \delta$.

$$f_4 = R - \frac{\sin\delta(p + q_f)}{\sin(2\Omega - 2\xi - \delta)}, \tag{B6}$$

Let

$$\sin\alpha = \frac{\sin\delta}{\sin\phi},$$

so that for this kind of material, the failure surface has two different shapes in X, Y stress space in Figs. B4 and B5.

Approximation of failure surface

In order to formulate the problem as a linear programming problem, it is necessary to express the above failure conditions as a number of linear functions having the form

$$A_{xx}\sigma_{xx} + A_{yy}\sigma_{yy} + 2A_{xy}\sigma_{xy} \leqslant G. \tag{B7}$$

This form is chosen because if the coordinate axes are transformed so that

$$\begin{bmatrix} \sigma_{ss} & \sigma_{st} \\ \sigma_{st} & \sigma_{tt} \end{bmatrix} = \begin{bmatrix} \cos\theta & \sin\theta \\ -\sin\theta & \cos\theta \end{bmatrix} \begin{bmatrix} \sigma_{xx} & \sigma_{xy} \\ \sigma_{xy} & \sigma_{yy} \end{bmatrix} \begin{bmatrix} \cos\theta & -\sin\theta \\ \sin\theta & \cos\theta \end{bmatrix}$$

then the linear function (B7) becomes

$$A_{ss}\sigma_{ss} + A_{tt}\sigma_{tt} + 2A_{st}\sigma_{st} \leqslant G$$

where

$$\begin{bmatrix} A_{ss} & A_{st} \\ A_{st} & A_{tt} \end{bmatrix} = \begin{bmatrix} \cos\theta & \sin\theta \\ -\sin\theta & \cos\theta \end{bmatrix} \begin{bmatrix} A_{xx} & A_{xy} \\ A_{xy} & A_{yy} \end{bmatrix} \begin{bmatrix} \cos\theta & -\sin\theta \\ \sin\theta & \cos\theta \end{bmatrix}$$

and where θ is the angle between the x-axis and the s-axis.

It will be assumed that a zero stress state is always safe and thus, that $G \geqslant 0$. A key assumption in the derivation of the limit theorem is that the failure surface is convex and so the approximating failure surface must also be convex.

Failure of fissures

Single set of fissures. For a material with a single set of fissures, as defined by (B3), failure on the fissures corresponds to two linear failure functions, viz

$$A^{(1)}_{xx}\sigma_{xx} + A^{(1)}_{yy}\sigma_{yy} + 2A^{(1)}_{xy}\sigma_{xy} \leqslant G^{(1)}$$

$$A^{(2)}_{xx}\sigma_{xx} + A^{(2)}_{yy}\sigma_{yy} + 2A^{(2)}_{xy}\sigma_{xy} \leqslant G^{(2)} \tag{B8}$$

with

$$A^{(1)}_{xx} = -\frac{1}{\sin\alpha}\left[\sin(2\xi+\delta) + \sin\delta\right],$$

$$A^{(1)}_{yy} = \frac{1}{\sin\alpha}\left[\sin(2\xi+\delta) - \sin\delta\right],$$

$$A^{(1)}_{xy} = \frac{1}{\sin\alpha}\cos(2\xi+\delta),$$

$$G^{(1)} = 2c_f\cos\delta,$$

$$A^{(2)}_{xx} = \frac{1}{\sin\alpha}\left[\sin(2\xi-\delta) - \sin\delta\right],$$

$$A^{(2)}_{yy} = -\frac{1}{\sin\alpha}\left[\sin(2\xi-\delta) + \sin\delta\right],$$

$$A^{(2)}_{xy} = -\frac{1}{\sin\alpha}\cos(2\xi-\delta),$$

$$G^{(2)} = 2c_f \cos\delta. \tag{B9}$$

These failure surfaces are already in a linear form and need no approximation.

Two sets of fissures. For a material with two sets of fissures, as defined in (B5), failure on the fissures corresponds to four linear failure functions:

$$A^{(i)}_{xx}\sigma_{xx} + A^{(i)}_{yy}\sigma_{yy} + 2A^{(i)}_{xy}\sigma_{xy} \leqslant G^{(i)}, \quad i = 1, 2, 3, 4,$$

where $A^{(i)}_{xx}$, $A^{(i)}_{yy}$, $A^{(i)}_{xy}$, $G^{(i)}$, $(i = 1, 2)$ are defined by (B9), and $A^{(i)}_{xx}$, $A^{(i)}_{yy}$, $A^{(i)}_{xy}$, G^{i} $(i = 3, 4)$ are defined by:

$$A^{(3)}_{xx} = \frac{1}{\sin\alpha}\left[\sin(2\xi + \delta) - \sin\delta\right],$$

$$A^{(3)}_{yy} = -\frac{1}{\sin\alpha}\left[\sin(2\xi + \delta) + \sin\delta\right],$$

$$A^{(3)}_{xy} = -\frac{1}{\sin\alpha}\cos(2\xi + \delta),$$

$$G^{(3)} = 2c_f \cos\delta,$$

$$A^{(4)}_{xx} = -\frac{1}{\sin\alpha}\left[\sin(2\xi - \delta) + \sin\delta\right],$$

$$A^{(4)}_{yy} = \frac{1}{\sin\alpha}\left[\sin(2\xi - \delta) - \sin\delta\right],$$

$$A^{(4)}_{xy} = \frac{1}{\sin\alpha}\cos(2\xi - \delta),$$

$$G^{(4)} = 2c_f \cos\delta. \tag{B10}$$

Again, these failure surfaces are already in a linear form and need no approximation.

Failure in the material matrix

For failure in the matrix, there are two kinds of approximations: an interior and an exterior approximation.

Interior approximation. In examining lower bound problems, the approximation of the failure surface needs to be interior. Suppose that this approximation consists of a number of triangular faces which are convex and contain the origin. If the three vertices of the triangle j (which are assumed to be non-collinear) are $(\sigma^{(1)}_{xx}, \sigma^{(1)}_{yy}, \sigma^{(1)}_{xy})$, $(\sigma^{(2)}_{xx}, \sigma^{(2)}_{yy}, \sigma^{(2)}_{xy})$, $(\sigma^{(3)}_{xx}, \sigma^{(3)}_{yy}, \sigma^{(3)}_{xy})$, then the failure surface has the equation:

$$\begin{vmatrix} \sigma_{xx} & \sigma_{yy} & \sigma_{xy} & 1 \\ \sigma_{xx}^{(1)} & \sigma_{yy}^{(1)} & \sigma_{xy}^{(1)} & 1 \\ \sigma_{xx}^{(2)} & \sigma_{yy}^{(2)} & \sigma_{xy}^{(2)} & 1 \\ \sigma_{xx}^{(3)} & \sigma_{yy}^{(3)} & \sigma_{xy}^{(3)} & 1 \end{vmatrix} = A_{xx}^{(j)}\sigma_{xx} + A_{yy}^{(j)}\sigma_{yy} + 2A_{xy}^{(j)}\sigma_{xy} - G^{(j)} = 0,$$

where

$$A_{xx}^{(j)} = \begin{vmatrix} \sigma_{yy}^{(1)} & \sigma_{xy}^{(1)} & 1 \\ \sigma_{yy}^{(2)} & \sigma_{xy}^{(2)} & 1 \\ \sigma_{yy}^{(3)} & \sigma_{xy}^{(3)} & 1 \end{vmatrix},$$

$$A_{yy}^{(j)} = \begin{vmatrix} \sigma_{xy}^{(1)} & \sigma_{xx}^{(1)} & 1 \\ \sigma_{xy}^{(2)} & \sigma_{xx}^{(2)} & 1 \\ \sigma_{xy}^{(3)} & \sigma_{xx}^{(3)} & 1 \end{vmatrix},$$

$$2A_{xy}^{(j)} = \begin{vmatrix} \sigma_{xx}^{(1)} & \sigma_{yy}^{(1)} & 1 \\ \sigma_{xx}^{(2)} & \sigma_{yy}^{(2)} & 1 \\ \sigma_{xx}^{(3)} & \sigma_{yy}^{(3)} & 1 \end{vmatrix},$$

$$G^{(j)} = \begin{vmatrix} \sigma_{xx}^{(1)} & \sigma_{yy}^{(1)} & \sigma_{xy}^{(1)} \\ \sigma_{xx}^{(2)} & \sigma_{yy}^{(2)} & \sigma_{xy}^{(2)} \\ \sigma_{xx}^{(3)} & \sigma_{yy}^{(3)} & \sigma_{xy}^{(3)} \end{vmatrix}.$$

For a Mohr–Coulomb material, it is convenient to introduce a Mohr representation of the stress, i.e.

$$\sigma_{xx}^{(1)} = p^{(1)} + R^{(1)}\cos 2\Omega^{(1)},$$

$$\sigma_{yy}^{(1)} = p^{(1)} - R^{(1)}\cos 2\Omega^{(1)},$$

$$\sigma_{xy}^{(1)} = R^{(1)}\sin 2\Omega^{(1)},$$

$$R^{(1)} = p^{(1)}\sin\phi + c\cos\phi,$$

$$\sigma_{xx}^{(2)} = p^{(2)} + R^{(2)}\cos 2\Omega^{(2)},$$

$$\sigma_{yy}^{(2)} = p^{(2)} - R^{(2)}\cos 2\Omega^{(2)},$$

$$\sigma_{xy}^{(2)} = R^{(2)} \sin 2\Omega^{(2)},$$

$$R^{(2)} = p^{(2)} \sin \phi + c \cos \phi,$$

$$\sigma_{xx}^{(3)} = -c \cos \phi,$$

$$\sigma_{yy}^{(3)} = -c \cos \phi,$$

$$\sigma_{xy}^{(3)} = 0.$$

By choosing the special points on the surface, viz assume that $p^{(1)} = p^{(2)} = p$, then

$$A_{xx}^{(j)} = \frac{\cos\left(\Omega^{(1)} + \Omega^{(2)}\right)}{\cos\left(\Omega^{(1)} - \Omega^{(2)}\right)} - \sin \phi,$$

$$A_{yy}^{(j)} = -\frac{\cos\left(\Omega^{(1)} + \Omega^{(2)}\right)}{\cos\left(\Omega^{(1)} - \Omega^{(2)}\right)} - \sin \phi,$$

$$A_{xy}^{(j)} = \frac{\sin\left(\Omega^{(1)} + \Omega^{(2)}\right)}{\cos\left(\Omega^{(1)} - \Omega^{(2)}\right)},$$

$$G^{(j)} = 2c \cos \phi, \quad j = 1,2,\ldots, J, \tag{B11}$$

where J is the number of the triangles to approximate the Mohr–Coulomb failure surface.

Exterior approximation. For the upper bound theorem, it is necessary to employ an exterior approximation. This can be done by selecting a number of sample points on the surface and determining their tangential planes. Thus, if $(\sigma_{xx}^{(i)}, \sigma_{yy}^{(i)}, \sigma_{xy}^{(i)})$ is such a sample point, then its tangential plane is defined by

$$A_{xx}^{(i)}\sigma_{xx} + A_{yy}^{(i)}\sigma_{yy} + 2A_{xy}^{(i)}\sigma_{xy} - G^{(i)} = 0$$

where

$$A_{xx}^{(i)} = \frac{\partial}{\partial \sigma_{xx}} f\left(\sigma_{xx} = \sigma_{xx}^{(i)}, \sigma_{yy} = \sigma_{yy}^{(i)}, \sigma_{xy} = \sigma_{xy}^{(i)}\right),$$

$$A_{yy}^{(i)} = \frac{\partial}{\partial \sigma_{yy}} f\left(\sigma_{xx} = \sigma_{xx}^{(i)}, \sigma_{yy} = \sigma_{yy}^{(i)}, \sigma_{xy} = \sigma_{xy}^{(i)}\right),$$

$$2A_{xy}^{(i)} = \frac{\partial}{\partial \sigma_{xy}} f\left(\sigma_{xx} = \sigma_{xx}^{(i)}, \sigma_{yy} = \sigma_{yy}^{(i)}, \sigma_{xy} = \sigma_{xy}^{(i)}\right),$$

$$G = A_{xx}^{(i)}\sigma_{xx}^{(i)} + A_{yy}^{(i)}\sigma_{yy}^{(i)} + 2A_{xy}^{(i)}\sigma_{xy}^{(i)}.$$

For a Mohr–Coulomb material, it is easy to find that

$$A_{xx}^{(i)} = \cos 2\Omega^{(i)} - \sin\phi,$$

$$A_{yy}^{(i)} = -\cos 2\Omega^{(i)} - \sin\phi,$$

$$A_{xy}^{(i)} = \sin 2\Omega^{(i)},$$

$$G = 2c\cos\phi, \quad j = 1, 2, \ldots, J \tag{B12}$$

where J is the number of the sample points on the failure surface.

Appendix C: velocity discontinuity

The velocity discontinuity multiplier $\dot{\kappa}$ is introduced as a new feature in the upper bound formulation. Consider a plastic material deforming in plane strain and obeying a failure criterion, eqn (1), and an associated flow rule, eqn (9). The region shown in Fig. C1 includes an intense distortion in the deformation field.

As the thickness $z \to 0$, a velocity discontinuity may develop. In such a case it would be found that $(\partial u/\partial y) \to \infty$ and $(\partial v/\partial y) \to \infty$, and $\partial u/\partial x$, $\partial v/\partial x$ are bounded when $z \to 0$. It can thus be seen that $\dot{\lambda} \to \infty$ and $(\partial f/\partial\sigma_{xx}) \to 0$. (Because f is smooth, $\partial f/\partial\sigma_{ij}$ are bounded.) Now integrating through the thickness of the layer, it is found that

$$\Delta v = \Delta\dot{\lambda}\frac{\partial f}{\partial\sigma_{yy}}, \quad \Delta u = \Delta\dot{\lambda}\frac{\partial f}{\partial\sigma_{xy}}, \quad 0 = \Delta\dot{\lambda}\frac{\partial f}{\partial\sigma_{xx}}, \tag{C1}$$

where

$$\Delta\dot{\lambda} = \dot{\kappa} = \int_0^z \dot{\lambda}\,\mathrm{d}y \geqslant 0, \quad \Delta u = \int_0^z \frac{\partial u}{\partial y}\,\mathrm{d}y, \quad \Delta v = \int_0^z \frac{\partial v}{\partial y}\,\mathrm{d}y,$$

and thus,

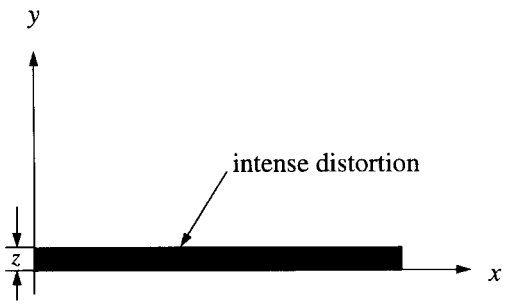

Fig. C1. Intensive distortion zone with thickness z.

$$\frac{\Delta v}{\Delta u} = \frac{\partial f/\partial \sigma_{yy}}{\partial f/\partial \sigma_{xy}}$$

where z is the thickness of the layer. The quantity $\dot{\kappa}$ is called the plastic discontinuity multiplier. The reason for this nomenclature will emerge as the quantity is developed when a discontinuity appears.

On such a velocity discontinuity we have

$$f(\sigma_{xx}, \sigma_{yy}, \sigma_{xy}) = 0, \quad \frac{\partial f}{\partial \sigma_{xx}}(\sigma_{xx}, \sigma_{yy}, \sigma_{xy}) = 0. \tag{C2}$$

When a discontinuity is parallel to the x-axis the failure surface is independent of σ_{xx} and the discontinuities only appear at the points in which (C2) holds. Therefore, for the purpose of calculation, the failure surface can be replaced by its tangential planes at the stress state being considered. These tangential planes are:

$$f_1 = \sigma_{xy} - \sigma_{yy} \tan \phi - c = 0,$$

$$f_2 = -\sigma_{xy} - \sigma_{yy} \tan \phi - c = 0. \tag{C3}$$

As a consequence, the flow rule at the discontinuity can be rewritten as

$$\dot{\varepsilon}_{xx} = \dot{\lambda}_1 \frac{\partial f_1}{\partial \sigma_{xx}} + \dot{\lambda}_2 \frac{\partial f_2}{\partial \sigma_{xx}},$$

$$\dot{\varepsilon}_{yy} = \dot{\lambda}_1 \frac{\partial f_1}{\partial \sigma_{yy}} + \dot{\lambda}_2 \frac{\partial f_2}{\partial \sigma_{yy}},$$

$$\dot{\gamma}_{xy} = \dot{\lambda}_1 \frac{\partial f_1}{\partial \sigma_{xy}} + \dot{\lambda}_2 \frac{\partial f_2}{\partial \sigma_{xy}}.$$

Hence, eqn (C1) can be written as

$$0 = \dot{\kappa}_1 \frac{\partial f_1}{\partial \sigma_{xx}} + \dot{\kappa}_2 \frac{\partial f_2}{\partial \sigma_{xx}},$$

$$\Delta v = \dot{\kappa}_1 \frac{\partial f_1}{\partial \sigma_{yy}} + \dot{\kappa}_2 \frac{\partial f_2}{\partial \sigma_{yy}} = -(\dot{\kappa}_1 - \dot{\kappa}_2) \tan \phi,$$

$$\Delta u = \dot{\kappa}_1 \frac{\partial f_1}{\partial \sigma_{xy}} + \dot{\kappa}_2 \frac{\partial f_2}{\partial \sigma_{xy}} = (\dot{\kappa}_1 - \dot{\kappa}_2), \tag{C4}$$

and the power dissipation in the discontinuous region is given by

$$P_d = \lim_{z \to 0} \int_0^z \int_l (\sigma_{xx}\dot{\varepsilon}_{xx} + \sigma_{yy}\dot{\varepsilon}_{yy} + \sigma_{xy}\dot{\gamma}_{xy}) \, \mathrm{d}x \, \mathrm{d}y = \int_l c(\dot{\kappa} + \dot{\kappa}) \, \mathrm{d}l \tag{C5}$$

where l is the length of the discontinuity, and the constraint equations at the discontinuity are given by

$$\Delta v = -(\dot{\kappa}_1 + \dot{\kappa}_2) \tan \phi,$$

$$\Delta u = (\dot{\kappa}_1 - \dot{\kappa}_2). \tag{C6}$$

References

Alehossein, H., Carter, J.P., Booker, J.R., 1992. Finite element analysis of rigid footings on jointed rock. In: Proc. COMPLAS III, Part 1. Pineridge Press, Barcelona, Spain, pp. 935–946.

Davis, E.H., 1980. Some plasticity solutions relevant to the bearing capacity of rock and fissured clay. J.C. Jaegar Memorial Lecture, Proc. 3rd A.N.Z. Conf. on Geomechanics, vol. 3. Wellington, New Zealand, pp. 27–36.

Drucker, D.C., Prager, W., Greenberg, J.H., 1951. Extended limit design theorems for continuous media. Q. Appl. Math 9, 381–389.

Lav, M.A., Carter, J.P., Booker, J.R., 1995. On the bearing capacity of clays. In: Proc. 14th Australasian Conf. on the Mechanics of Structures and Materials. Hobart, pp. 38–43.

Michalowski, R.L., 1993. Limit analysis of weak layers under embankment. Soils and Foundations 33, 155–168.

Sloan, S.W., 1980. Lower bound limit analysis using finite elements and linear programming. Int. J. Numer. Anal. Methods in Geomechanics 12, 61–77.

Sloan, S.W., Kleeman, P.W., 1996. Upper bound limit analysis using discontinuous velocity fields. Comput. Methods Appl. Mech. Eng 127, 293–314.

Yu, H.S., Sloan, S.W., 1997. Finite element limit analysis of reinforced soils. Computers and Structures 63, 567–577.

Zheng, X., Booker, J.R., 1997. Application of the theory of plasticity to analysis of bearing capacity problems in fissured materials. In: Aliabadi, M.H. (Eds.), Fracture of Rock. Computational Mechanics Publications, in press.